Optimized cross-resonance gate for coupled transmon systems

Susanna Kirchhoff,[1] Torsten Keßler,[1] Per J. Liebermann,[1,*] Elie Assémat,[1] Shai Machnes,[1] Felix Motzoi,[1,2] and Frank K. Wilhelm[1]

[1] *Theoretical Physics, Saarland University, 66123 Saarbrücken, Germany*
[2] *Department of Physics and Astronomy, Aarhus University, DK-8000 Aarhus C, Denmark*

(Dated: January 10, 2017)

The cross-resonant gate is an entangling gate for fixed frequency superconducting qubits introduced for untunable qubits. While being simple and extensible, it suffers from long duration and limited fidelity. Using two different optimal control algorithms, we probe the quantum speed limit for a CNOT gate in this system. We show that the ability to approach this limit depends strongly on the ansatz used to describe the optimal control pulse. A piecewise constant ansatz with a single carrier leads to an experimentally feasible pulse shape, shorter than the one currently used in experiments, but that remains relatively far from the speed limit. On the other hand, an ansatz based on the two dominant frequencies involved in the optimal control problem allows to generate an optimal solution more than twice as fast, in under 30ns. This comes close to the theoretical quantum speed limit, which we estimate at 15ns for typical circuit-QED parameters, which is more than an order of magnitude faster than current experimental microwave-driven realizations, and more than twice as fast as tunable direct-coupling experimental realizations.

arXiv:1701.01841v1 [quant-ph] 7 Jan 2017

I. INTRODUCTION

Circuit-QED is a promising technology for quantum computing. An important requirement for scalable operation of the architecture is high-accuracy implementation of two-qubit gates. A leading candidate for resonator-mediated interaction between a pair of superconducting qubits is the so-called cross-resonance (CR) gate [1–4] which has been implemented experimentally with over 99% average gate fidelity [5]. The CR gate functions by combining the frequency addressability of one qubit with the spatial addressability of a second, such that the the first qubit is driven by the control line of the second, i.e. "cross-resonantly". The design avoids the complexity and noise sources that are present via low-frequency magnetic (flux) tuning of the qubit-qubit interaction [6]. It also aims to improve on methods for high-frequency addressing of desired two-qubit transitions by utilizing the additional spatial addressability that comes from dedicated control circuitry.

The primary impediments to high-fidelity operation thus far have come from incoherent errors such as T_1 and T_2 effects and unitary errors such as crosstalk [7] and frequency crowding [8]. The main method to counteract the former is to shorten gate times as much as possible, but this can drastically increase unitary errors, especially from higher order corrections to the perturbative model of the gate mechanism.

In this article we systematically optimize the design of the CR gate to reduce the gate time as much as possible and numerically estimate the quantum speed limit (QSL) for the gate [9–11]. We employ a full Jaynes-Cummings model which eliminates many of the analytic simplifications that set bounds for an analysis of the gate in a deeply non adiabatic regime. Moreover, it is known that a careful analysis with regard to parameterization of the control sequence is required to tailor efficiently the pulse to the experimental constraints of the experimental aparatus [12]. However, the QSL depends on the constraints included in the optimization problem, and thus may also depend on the chosen parameterization of the control pulse. Therefore, we probe the relationship between the QSL and different physically meaningful parameterizations, which leads to a new understanding of the limitations of the original cross-resonant control scheme and to propose alternative control strategies.

This manuscript is organized as follows: Section II presents the theoretical model of the system; Section III introduces the numerical method; in Section IV we show that the unconstrained quantum speed limit is much shorter in duration than the existing strategy; Section V describes the first optimization results and point out the role of higher frequency components; Section VI studies the QSL with the Fourier parameterization of the drive shape; Section VII explains the influence of the bandwidth constraint and proposes two solutions; Finally, in Section VIII we make concluding remarks.

II. SYSTEM

Let us consider two transmon qubits coupled by a bus resonator. Each transmon is described as an anharmonic oscillator and the coupling to the resonator by an appropriately extended Jaynes-Cummings model [13–15]. The qubits consist in the first two levels of these two anharmonic oscillators. As in [5], we assume that σ_x, σ_y type controls are available. We further assume that the qubit frequencies can be calibrated by a quasi-static flux line. The aim of the latter is not to provide another time dependent control function, but to statically shift the qubit frequencies to a value more favorable to

* per@lusi.uni-sb.de

the optimization process. With the notations of [14], the Hamiltonian takes the form

$$H(t) = \omega_r a^\dagger a + \sum_{k=1}^{2} \Big(\omega_k b_k^\dagger b_k + \alpha_k b_k^\dagger b_k^\dagger b_k b_k + g_k (a b_k^\dagger + a^\dagger b_k) + \sum_{l=1}^{L} \mathcal{E}_{k,l}(t) \cos\left(\omega_{k,l}^d t + \phi_{k,l}\right) (b_k + b_k^\dagger) \Big) \quad (1)$$

where $a^\dagger$,$b_1^\dagger$ and $b_2^\dagger$ are the creation operators for the cavity and the two transmons respectively; g_k are the couplings between the resonator and the qubits; ω_r, ω_1 and ω_2 are the respective frequencies of the cavity and the two transmons; $\mathcal{E}_{k,l}$ are the low-frequency envelopes of the microwave drive and ω^d are the carrier frequencies of the L control drives with phase offset $\phi_{k,l}$. After moving to the rotating frame at the frequency of the first qubit and applying a rotating wave approximation, the Hamiltonian takes the form

$$H_{\text{rwa}}(t) = \Delta a^\dagger a + \sum_{k=1}^{2} \Big(g_k (a b_k^\dagger + a^\dagger b_k) + \delta_k b_k^\dagger b_k + \alpha b_k^\dagger b_k^\dagger b_k b_k + \mathcal{E}_k^x(t)(b_k + b_k^\dagger) + i\mathcal{E}_k^y(t)(b_k^\dagger - b_k) + f_k b_k^\dagger b_k \Big) , \quad (2)$$

where Δ is the detuning of the cavity from the principle (carrier) drive frequency of the controls and δ_k are the detunings of the transmons. f_k are used to optimize the latter, and can be thought of as the static flux tuning of the transmon frequencies and/or shifting of the principle drive frequency. The numerical simulations and optimizations presented below include the three first levels of the resonator and the three first levels of each transmon.

III. NUMERICAL METHOD

This work relies mainly on the optimal control algorithm Gradient Ascent Pulse Engineering – GRAPE [16]. It was developed to numerically determine the shape of the control function that maximizes a goal function. In the case of a gate generation problem, a possible goal function is

$$\Phi_{\text{goal}} = \frac{1}{N^2} \left| \text{Tr}\left(U_{\text{target}}^\dagger U(t_g) \right) \right|^2 , \quad (3)$$

where t_g is the target gate duration, N the dimension of the computational subspace and U the unitary evolution operator. For other examples of goal functions and in-depth study of optimal control algorithms, the interested reader may refer to [17].

The GRAPE algorithm considers a piecewise constant approximation of the control function. The values of all slices are stored in a vector whose size defines the search space dimension. At each iteration, GRAPE computes the gradient of the goal function with respect to the control function vector, then updates the control function vector based on this gradient. The first iteration starts with a guess of the control function. In many cases this guess is extremely important, especially when the target gate time is close to the quantum speed limit, where local minima tend to appear in the optimal control landscape [18].

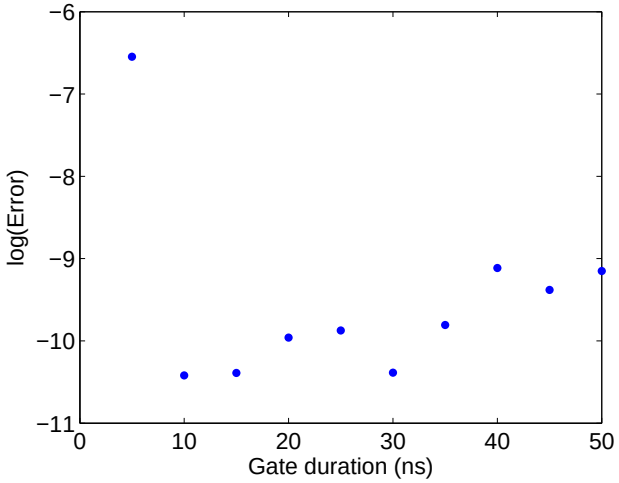

FIG. 1. Determination of the Quantum Speed Limit (QSL) using arbitrary amplitude piecewise constant controls with high sampling rate (≈ 0.1ns) and no filter.

IV. UNCONSTRAINED QUANTUM SPEED LIMIT

We first look for the QSL by using the least possible constrained parameterization, i. e. no amplitude bounds and high resolution, with 500 time slices for each gate duration t_g. Assuming that the parameterization is flexible enough, if a QSL is observed it comes from the physics of the system. One standard method to probe numerically the QSL is to plot a measure of the gate fidelity as function of the gate duration [15, 19]. For different gates time we ran many GRAPE optimization with different random guesses. The average final gate error, defined as $|1 - \Phi_{\text{goal}}|$ are shown in fig. 1. We observe a clear jump between 10ns and 15ns gate time that indicates the presence of a QSL. Interestingly this is more than an order of magnitude shorter than the gate time presented in [2]. However, because no constraint is included, these optimal control shapes are far from what can be experimentally implemented. Taking in account the constraints of the experiments will push the QSL towards a longer gate time, while remaining shorter than the original cross-resonance gate, as shown in the following.

TABLE I. Values of the parameters of the Hamiltonian 4 in GHz.

Parameter	Value in GHz
$\Delta/(2\pi)$	0.4
$g_1/(2\pi)$	0.1
$g_2/(2\pi)$	0.1
$\alpha/(2\pi)$	-0.32
$\delta_1/(2\pi)$	0.0
$\delta_2/(2\pi)$	-0.67

V. SEARCH FOR A MORE REALISTIC OPTIMAL CONTROL

In this work, the initial guess of a trial function for $\mathcal{E}^x$ is set here by following the cross resonant scheme implemented in [2] based on the effective interaction presented in [1]. A cross resonant drive on a two transmon system is a drive applied on one qubit such that the drive frequency is resonant with the second qubit. This scheme leads to generating a CNOT gate. Indeed, let us consider the effective coupling J_{eff} between the two qubits that quantifies the effective interaction mediated by the resonator. In the case where J_{eff} is small compared to the detuning δ_2 between the qubits, a drive at frequency $\tilde{\omega_2} = \omega_2 - (J_{\text{eff}})^2/\delta_2$ generates dynamics that can be described by an effective Hamiltonian of the form

$$H_{\text{eff}} = u_1^{\text{eff}} \sigma_1^z \otimes \sigma_2^x + u_2^{\text{eff}} \sigma_1^x \otimes \mathbb{1}\,, \tag{4}$$

where σ_i are the Pauli operators and u_i^{eff} denote the relative scaling of the effective interaction. The ZX interaction present in this effective Hamiltonian can generate directly a CNOT gate.

The performance of the initial guess is further improved by limiting the effect of the second term in Eq. 4. Here we assume this spectral constraint (suppressing the second term) can be satisfied by using a second off-phase quadrature $\mathcal{E}^y$ of the control envelope set proportional to the derivative of $\mathcal{E}^x$ and inversely proportional to the qubit frequency separation δ_2, as in the Derivative Removal by Adiabatic Gate (DRAG) method [7, 20].

These analytical techniques would not be sufficient to obtain high fidelity gate with the model at hand due to the complexity of the levels structure. However, the initial guess should be relevant enough to be located in the basins of attraction of a higher fidelity solution, which allows the GRAPE algorithm to converge.

Following this direction, the first optimization attempt was carried out with the following initial control functions:

$$\begin{aligned}
&\mathcal{E}_1^x(t) = 0 \quad \mathcal{E}_1^y(t) = 0 \\
&\mathcal{E}_2^x(t) = 0.4 \exp\left(-\frac{(t-\mu)^2}{2\sigma^2}\right) \quad \mu = \frac{t_g}{2},\, \sigma = \frac{t_g}{4} \\
&\mathcal{E}_2^y(t) = \frac{1}{\delta_2}\dot{\mathcal{E}}_1^x(t)\,, \quad f_1 = 0\,, \quad f_2 = 0.1\,,
\end{aligned} \tag{5}$$

where the amplitude are given in GHz and f_1 and f_2 are respectively constant but tunable frequency offsets of qubit 1 and 2 from the drive frequency. Here, we include in the optimization a bound on the control amplitude and a lower sampling rate (time slices of 0.2 ns). The minimum gate time threshold for possible convergence is found to be $t_g = 27$ ns. As expected, this is longer than the physical QSL, but still much shorter than the 180ns original CR gate. The initial and final drive shapes are shown in fig. 2. We observe that the strong cross-resonant drive remains after the optimization, which indicates that the CR scheme is still the main physical mechanism in play. Although the pulse involves a complicated sequence of maneuvers to obtain high-fidelity at a very short time, it is nonetheless very promising as it implies the possibility of reducing gate operation time by an order of magnitude [5], reducing the leading sources of decoherence by a similar fraction, and even outperforming gate times with tunable qubit frequency architectures [21].

VI. QUANTUM SPEED LIMIT WITH THE FOURIER ANSATZ

Another important feature of quantum control sequences is that they can be parametrized with as small as possible a number of controls. This simplicity can greatly aid in analytical, numerical, and experimental reproducibility of the solution, and avoid getting stuck in local minima due to miscallibration. For these purposes we use a parameterization based on the number of Fourier components of the pulse, though any other set of parameters more appropriate for the given control task could have been substituted. Each control is parametrized by a truncated Fourier series that is fed to a sum of two sigmoids to enforce the global bound and a smooth start and finish. The amplitude coefficients, frequencies and phases are optimized with the GOAT algorithm [12], a recent gradient base algorithm that allows to handle analytic ansatzes more efficiently than GRAPE.

We first start with a large number of Fourier components and probe the QSL. The number of components is chosen to offer roughly the same number of parameters to describe the drive shape as we had in the piecewise constant case of Fig. 1. We observe in Fig. 3 that the QSL is less sharp than what was observed with the piecewise constant description, which illustrates the clear influence of the choice of the control representation on the control

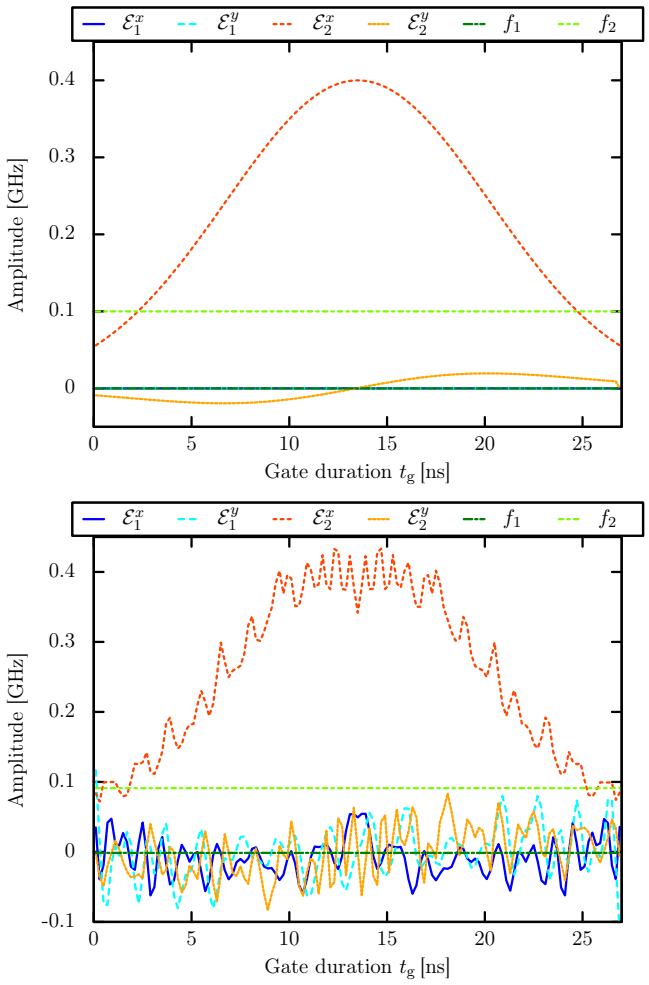
$\mathcal{E}_1^x$ $\mathcal{E}_1^y$ $\mathcal{E}_2^x$ $\mathcal{E}_2^y$ f_1 f_2
Amplitude [GHz]
Gate duration t_g [ns]
$\mathcal{E}_1^x$ $\mathcal{E}_1^y$ $\mathcal{E}_2^x$ $\mathcal{E}_2^y$ f_1 f_2
Amplitude [GHz]
Gate duration t_g [ns]

FIG. 2. Preliminary, high-bandwidth optimization of the drive functions. Top: initial control guesses. Bottom: optimized controls with $\Phi_{\text{goal}} = 0.998$. The average structure of the initial guess remains after the optimization which validates the CR scheme.

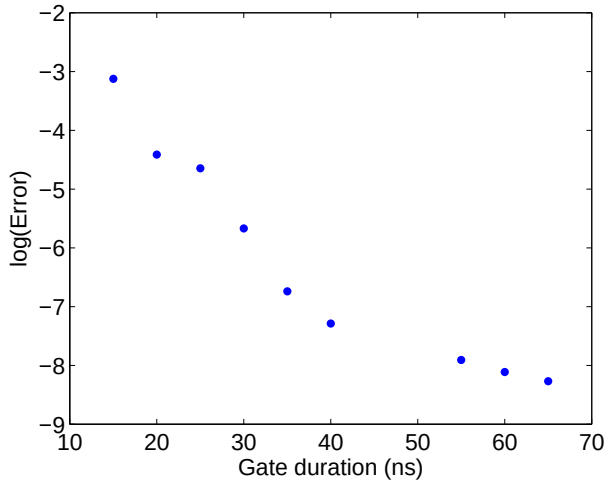

FIG. 3. Determination of the Quantum Speed Limit (QSL) using 167 Fourier components per control. The choice of parameterization of the drive shape has a clear influence on the QSL, when compared to Fig. 1.

landscape. Then, we iteratively remove the component with the smallest amplitude and reoptimize, down to only 9 components. However, this reduction is at the cost of an increased gate time of 70ns and the appearance of some very high frequencies. This offers a hint to explain why the unconstrained piecewise optimization manages to converge to a gate error of 10^{-10}, whereas the spectral optimization with a smaller frequency range converged only to 10^{-3}. It seems that high frequency components are necessary for the fine tuning needed to achieve a high accuracy. Moreover, this could also be a sign that the Fourier ansatz is not the most efficient for this system, and one may wish to try a few other analytic ansatz. The GOAT package would be well suited for such study.

Nonetheless, using 167 Fourier components we find that the minimum time is around 15ns to obtain 0.001 error, which is consistent with the piecewise-constant case, and thus indicates this is probably as fast as we can expect to do in this typical regime of control parameters, regardless of the chosen control parameterization. We find relatively short gate times even with just 9 Fourier components per control, which is far fewer parameters than the approximately 200 time steps used in the piecewise-constant parameterization. This is a significant reduction in the number of parameters, but such optimal control shapes require increased experimental overhead compared to current state-of-the-art experimental setups, which usually only employ at most a handful of carrier frequencies at a time.

VII. INFLUENCE OF THE BANDWIDTH CONSTRAINT AND WORKAROUND

The piecewise constant parameterization with high resolution controls provides a theoretic lower bound to gate times, but for time resolved optimization we are in practice limited by the AWG's time resolution. Furthermore, the applied control from the AWG usually undergoes some filtering. Here we optimize the pulses for an AWG with finite time resolution of 1 ns, fine steps of 0.2 ns, buffers of 4 ns duration at the beginning and the end, and filtering of the signal, see [22] for details. The filtering is applied via a Gaussian window function with standard deviation $\sigma = 0.4$ ns, i.e., a bandwidth of 331 MHz. For a gate time of 70 ns, a GRAPE optimization generates the controls and spectrum shown in Fig. 4 with a fidelity of 99.9%. The filtering process leads to slower optimization and forces the use of longer gate times to obtain higher fidelities. Nonetheless, this optimal drive shape includes all relevant constraints and could be directly implemented in an experiment. A remaining step would be to tune it to the unknown exact values of the

system parameters, with possibly additional closed-loop tuning or optimization [23].

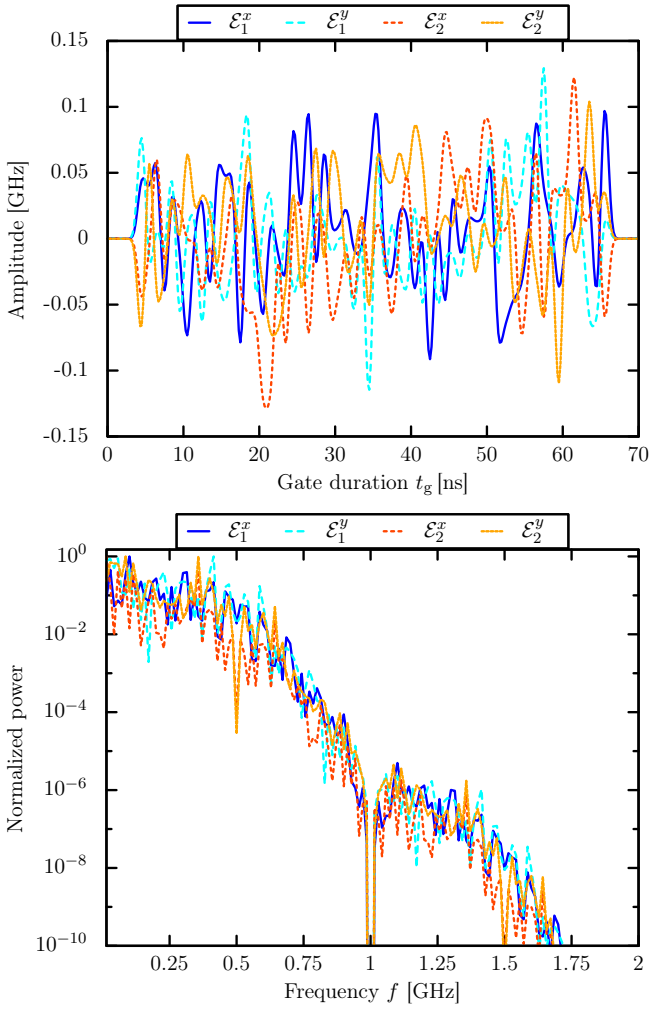

FIG. 4. Pulse shapes and spectrum of the optimal drive shape for filtered PWC ansatz with gate time of 70 ns and 99.9% fidelity. The flux is not optimized here.

To further decrease the experimental overhead and facilitate its calibration, we further constrain the waveform based on the primary frequencies found in the initial optimization and limit to the primary three frequency components, with time-domain control of each waveform within the bandwidth limit of each of the three frequencies.

The spectra of the controls are dominated by the frequencies 0.47GHz, 0.57GHz and 0.67GHz. The 0.57GHz corresponds to the frequency of the second qubit shifted by f_2, while 0.47GHz and 0.67GHz can be interpreted as the influence of the Rabi splitting on the control process. Thus, we choose

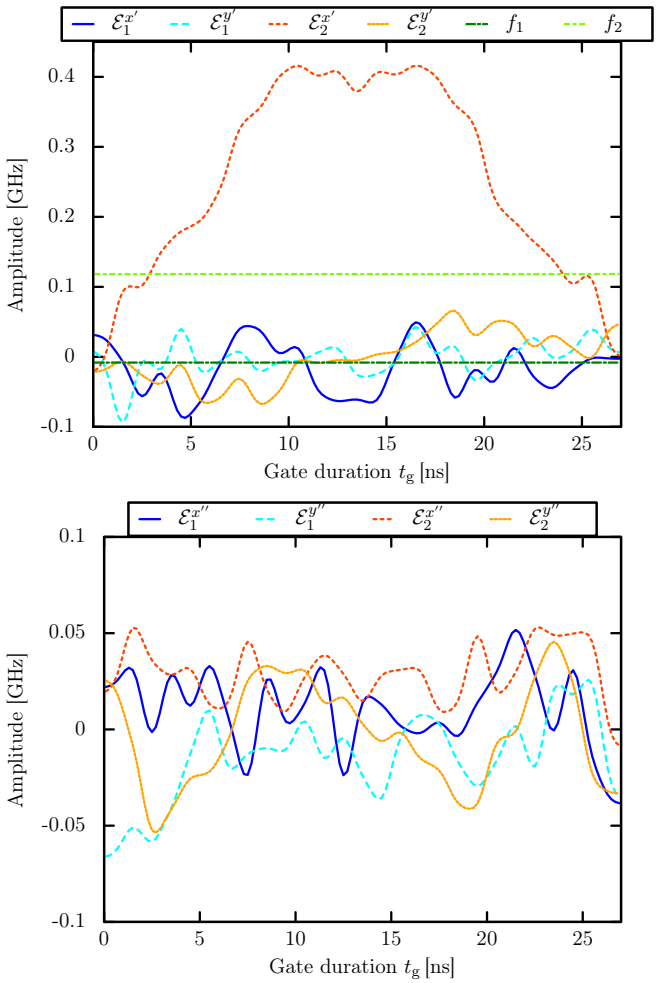

FIG. 5. Final optimization of the control functions. Top: controls at qubit 1 frequency. Bottom: controls at qubit 2 frequency.

$$
\begin{aligned}
\mathcal{E}_1^x(t) &= \mathcal{E}_1^{x'}(t) + \cos((\delta+2g)t)\mathcal{E}_1^{x''}(t) \\
\mathcal{E}_1^y(t) &= \mathcal{E}_1^{y'}(t) + \cos((\delta+2g)t)\mathcal{E}_1^{y''}(t) \\
\mathcal{E}_2^x(t) &= \mathcal{E}_2^{x'}(t) + \cos(\delta t)\mathcal{E}_2^{x''}(t) \\
\mathcal{E}_2^y(t) &= \mathcal{E}_2^{y'}(t) + \cos(\delta t)\mathcal{E}_2^{y''}(t)
\end{aligned} \tag{6}
$$

where the quotes symbols denote the new control functions and $\delta = \delta_2 - f_2$ is the qubit separation. This doubles the number of functions to optimize but their smoother behaviour improves the convergence speed nonetheless. Moreover, a Gaussian filter with a bandwith of 331 MHz is added to account for the distortion of the piecewise-constant control functions by waveform generators [22]. In an experiment, this would require two carrier frequencies, one for each qubit. The first one would shape the terms $\mathcal{E}_i^{n'}$ and the second one would shape the terms $\mathcal{E}_i^{n''}$. This should be feasible with current technology, the only remaining issue would be the calibration of the optimal

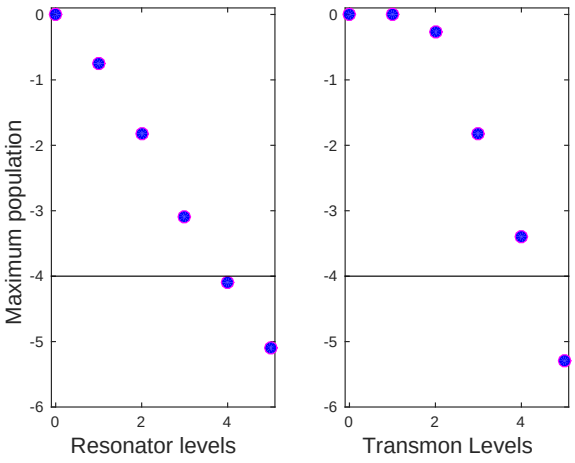

FIG. 6. Maximum transient Log(population) leakage in the higher levels of the resonator (left) and the transmons (right) during a dynamics driven by the optimal controls.

pulse in the experiment, see [12, 23] for an in depth discussion of this matter.

The optimization is carried out with coarse pixels of 1 ns and a fine time step of 0.2 ns and reaches a final fidelity of 0.99. The control functions optimized $\mathcal{E}_j^{i'}$, $\mathcal{E}_j^{i''}$ and f_j are shown in figure 5. Note the approximate time symmetry of the control function $\mathcal{E}_2^{x'}$, reminiscent of the Hahn echo pulses used in nuclear magnetic resonance. The constant value of the frequency detuning is also optimized but its value appears to be stuck in a local minimum and does not evolve significantly during the optimizations.

To test the validity of the truncation of the Hilbert space, the optimal control functions were applied to a larger space including 5 levels of the resonator and each transmon. The maximum population reached during the dynamics by each level is plotted in Fig. 6. For the transmons, the maximum is also taken over the two transmons: $M_r = \log[\max_t(p_r(t))]$ and $M_{\text{Transmons}} = \log[\max_{t;i\in 1,2}(p_{r_i}(t))]$. The population of the fourth level of the resonator and transmons remain below 10^{-3} while the transmons populate their fourth level up to 10^{-2}. This is sufficient for the accuracy aimed in this work, however, further optimization on the transmon populations would be necessary for high accuracy applications.

VIII. CONCLUSIONS

We have explored numerically the quantum speed limit of the Cross-Resonance gate using the algorithms GRAPE and GOAT. We showed that the physical quantum speed limit is more than an order of magnitude smaller than the gate duration currently used, approximately $10 - 15$ns for typical circuit-QED parameters. However, to reach this limit a high resolution is required. Two intermediate solutions were proposed. The first uses a single frequency resonant with the driven transition and generates a realistic control shape with a gate duration of 70ns, far from the quantum speed limit but that still represent a significant improvement over existing control shapes. The second implies to shape independently two different carrier frequencies resonant respectively with the two qubits. This should be feasible with existing hardware and it would allow to reach a gate time of 27ns, or just above the quantum speed limit.

ACKNOWLEDGMENTS

E.A. acknowledges support from the Alexander von Humboldt Foundation. S.K. and S.M. acknowledges funding from the IARPA through the LogiQ grant No. W911NF-16-1-0114. P.J.L. and F.K.M. acknowledges support from the European Union through the ScaleQIT project.

[1] G. S. Paraoanu, Phys. Rev. B **74**, 140504 (2006).
[2] J. M. Chow, A. D. Córcoles, J. M. Gambetta, C. Rigetti, B. R. Johnson, J. A. Smolin, J. R. Rozen, G. A. Keefe, M. B. Rothwell, M. B. Ketchen, and M. Steffen, Phys. Rev. Lett. **107**, 080502 (2011).
[3] J. M. Chow, J. M. Gambetta, A. D. Córcoles, S. T. Merkel, J. A. Smolin, C. Rigetti, S. Poletto, G. A. Keefe, M. B. Rothwell, J. R. Rozen, M. B. Ketchen, and M. Steffen, Phys. Rev. Lett. **109**, 060501 (2012).
[4] J. M. Chow, J. M. Gambetta, E. Magesan, D. W. Abraham, A. W. Cross, B. R. Johnson, N. A. Masluk, C. A. Ryan, J. A. Smolin, S. J. Srinivasan, and M. Steffen, Nat. Commun. **5**, 4015 (2014).
[5] S. Sheldon, E. Magesan, J. M. Chow, and J. M. Gambetta, Phys. Rev. A **93**, 060302 (2016).
[6] J. Koch, T. M. Yu, J. Gambetta, A. A. Houck, D. I. Schuster, J. Majer, A. Blais, M. H. Devoret, S. M. Girvin, and R. J. Schoelkopf, Phys. Rev. A **76**, 042319 (2007).
[7] F. Motzoi and F. K. Wilhelm, Phys. Rev. A **88**, 062318 (2013).
[8] L. S. Theis, F. Motzoi, and F. K. Wilhelm, Phys. Rev. A **93**, 012324 (2016).
[9] L. B. Levitin and T. Toffoli, Phys. Rev. Lett. **103**, 160502 (2009).
[10] M. Lapert, Y. Zhang, M. Braun, S. J. Glaser, and D. Sugny, Phys. Rev. Lett. **104**, 083001 (2010).
[11] T. Caneva, M. Murphy, T. Calarco, R. Fazio, S. Montangero, V. Giovannetti, and G. E. Santoro, Phys. Rev. Lett. **103**, 240501 (2009).
[12] S. Machnes, D. J. Tannor, F. K. Wilhelm, and E. Assémat, "Gradient optimization of analytic controls: the route to high accuracy quantum optimal control," (2015).

[13] C. Rigetti, J. M. Gambetta, S. Poletto, B. L. T. Plourde, J. M. Chow, A. D. Córcoles, J. A. Smolin, S. T. Merkel, J. R. Rozen, G. A. Keefe, M. B. Rothwell, M. B. Ketchen, and M. Steffen, Phys. Rev. B **86**, 100506 (2012).

[14] A. Cross and J. Gambetta, Phys. Rev. A **91**, 032325 (2015).

[15] D. J. Egger and F. K. Wilhelm, Supercond. Sci. Technol. **27**, 014001 (2014).

[16] N. Khaneja, T. Reiss, C. Kehlet, T. Schulte-Herbrüggen, and S. J. Glaser, J. Magn. Reson. **172**, 296 (2005).

[17] S. Machnes, U. Sander, S. J. Glaser, P. de Fouquières, A. Gruslys, S. Schirmer, and T. Schulte-Herbrüggen, Phys. Rev. A **84**, 022305 (2011), software avaibable at qlib.info.

[18] N. Rach, M. M. Müller, T. Calarco, and S. Montangero, Phys. Rev. A **92**, 062343 (2015).

[19] J. J. W. H. Sørensen, M. K. Pedersen, M. Munch, P. Haikka, J. H. Jensen, T. Planke, M. G. Andreasen, M. Gajdacz, K. Mølmer, A. Lieberoth, and J. F. Sherson, Nature **532**, 210 (2016).

[20] F. Motzoi, J. M. Gambetta, P. Rebentrost, and F. K. Wilhelm, Phys. Rev. Lett. **103**, 110501 (2009).

[21] J. Kelly, R. Barends, A. G. Fowler, A. Megrant, E. Jeffrey, T. C. White, D. Sank, J. Y. Mutus, B. Campbell, Y. Chen, Z. Chen, B. Chiaro, A. Dunsworth, I.-C. Hoi, C. Neill, P. J. J. O/'Malley, C. Quintana, P. Roushan, A. Vainsencher, J. Wenner, A. N. Cleland, and J. M. Martinis, Nature **519**, 66 (2015).

[22] F. Motzoi, J. M. Gambetta, S. T. Merkel, and F. K. Wilhelm, Phys. Rev. A **84**, 022307 (2011).

[23] D. J. Egger and F. K. Wilhelm, Phys. Rev. Lett. **112**, 240503 (2014).